



HAL
open science

Experimental and numerical analysis of unfolding failure of L-shaped CFRP specimens

Pierre Journoud, Christophe Bouvet, Bruno Castanié, Frédéric Laurin, Léon Ratsifandrihana

► To cite this version:

Pierre Journoud, Christophe Bouvet, Bruno Castanié, Frédéric Laurin, Léon Ratsifandrihana. Experimental and numerical analysis of unfolding failure of L-shaped CFRP specimens. *Composite Structures*, 2019, 232, 111563, p. 1-13. 10.1016/j.compstruct.2019.111563 . hal-02382912

HAL Id: hal-02382912

<https://hal.science/hal-02382912v1>

Submitted on 27 Nov 2019

HAL is a multi-disciplinary open access archive for the deposit and dissemination of scientific research documents, whether they are published or not. The documents may come from teaching and research institutions in France or abroad, or from public or private research centers.

L'archive ouverte pluridisciplinaire **HAL**, est destinée au dépôt et à la diffusion de documents scientifiques de niveau recherche, publiés ou non, émanant des établissements d'enseignement et de recherche français ou étrangers, des laboratoires publics ou privés.

Experimental and numerical analysis of unfolding failure of L-Shaped CFRP specimens

P. Journoud^{1,2}, C. Bouvet¹, B. Castanié¹, F. Laurin³, L. Ratsifandrihana²

1: Institut Clément Ader, Université de Toulouse, CNRS UMR 5312 – INSA – ISAE-SUPAERO – IMT Mines Albi – UPS – 3 rue Caroline Aigle, 31400 TOULOUSE, FRANCE

2 : Segula Aerospace & Defence, Segula Technologie – immeuble EQUINOX – bat. 1, 24 Boulevard Déodat de Severac, 31770 COLOMIERS, FRANCE

3 : ONERA – 29 avenue de la Division Leclerc, 92322 CHATILLON, FRANCE

Abstract

Highly curved laminated parts are used at the junction between two different perpendicular panels on aircraft primary structures. Usually, these laminates fail by delamination due to a bending moment, which appears when the part is loaded. The bending moment tries to flatten the part and out-of-plane tensile stresses are generated in the curvature. This failure is traditionally called unfolding failure. The modelling strategy called the ‘Discrete Ply Model’ (DPM) is used to simulate four-point bending tests on L-angle specimens. Experimental results of four point bending tests carried out at ONERA are used to validate the approach. Four different stacking sequences with the same thickness are taken into consideration in this study. In a second part, a sensitivity analysis on frictional coefficient, intralaminar matrix cracking, transverse tensile and shearing strength, and critical energy release rate in modes I and II is performed numerically and provides an original explanation of the failure scenario and the most influential parameter.

Keywords: composite L-angle, unfolding failure, translaminar matrix cracking, delamination

1. Introduction

In today's global warming context, airline companies want lighter airplanes and, in these circumstances, composite laminates are largely used for the interesting ratio between their weight and mechanical properties. Composite laminates are no longer only used for flat components but are also common for components with high curvatures. Composite L-angles are especially used at the junction between two perpendicular parts, such as the frame and fuselage, in parts called "clips". Most of the time, they are subjected to bending moments, which try to flatten the curvature and induce out-of-plane stresses, which then lead to unfolding failures.

So, more generally, unfolding failure is commonly identified in highly-curved laminates [1,2]. Usually the propagation of intralaminar matrix cracking and delamination are prompted in L-angle specimens and cause the final failure. A precise stress analysis is necessary to determine the stress state in the curved part of the specimen and the use of a failure criterion permits the failure onset to be assessed and the failure strength of the curved composite laminates to be evaluated.

A two-dimensional solution has been developed by Lekhnitskii et al. [3] for homogeneous anisotropic curved beams under bending moments and end load. It allows for the calculation of interlaminar stresses. In the literature, approximating the laminate by a homogenous equivalent material is largely used to apply the previous solution [4–7]. Nevertheless, the non-homogeneity induced by stacking sequences considerably affects the maximum interlaminar normal stress (INS) and the interlaminar stress distribution. These effects are not taken into account by Lekhnitskii's approach. That is why Ko and Jackson [8] developed an extension for laminate materials. Then González-Cantero et al. [9] developed a model that takes the curvature of the specimen into consideration and permits loads distributed over the curved laminate to be calculated.

In the case of L-shaped beams, the change of curvature at the junction between the straight arms and the curved part induces non-regularized stresses. The models presented above are not able to take this effect into consideration, as exposed by Most et al. [10]. González-Cantero et al. [11,12] extended their model to allow these non-regularized stresses. The stress state of the curved part may have been impacted by three-dimensional effects. By using a finite element model (FEM) and a fine mesh refinement, it is possible to obtain a better stress state through the thickness of L-angle specimens.

It is necessary to have a precise stress state to determine the unfolding failure onset by means of failure criteria. Orifici et al. [13] reviewed the different delamination criteria of the literature. Among these, the Kim and Soni criterion [14] is one of the most commonly used; Brewer and Lagacé [15] developed a criterion similar to the previous one. Their criterion makes a distinction between tensile and compressive

zones of the interlaminar normal stresses. Wisnom et al. [16] developed another delamination criterion, which considers the matrix stress in all directions. Interlaminar shear strength and interlaminar tensile strength are required for these failure criteria. A three-point bending test [17] is used to find the interlaminar shear strength, while, most of the time, the interlaminar tensile strength is obtained by a four-point bending test [18], initially proposed by Jackson [19]. Nevertheless, it is possible to use the three-point bending test with a stacking sequence along the axial direction of the test [20] or use the tensile test in the interlaminar direction [21,22] to obtain the interlaminar tensile strength.

The four-point bending test has been standardized [18] for unidirectional laminate composites. It calculates the bending moment at the first peak load from the applied loading and the geometry of the specimen. This corresponds to the onset of delamination and the bending moment is defined as the curved beam strength (CBS). Once the CBS is calculated, it is possible to determine the interlaminar tensile strength from Kedward's estimation of the maximum of interlaminar normal stress [2] but only for specimens with all plies at 0° , defining the along-the-length direction of the specimen.

Edwards and Thompson [23] highlight a thickness dependence of the interlaminar tensile strength calculated from the CBS, for other stacking sequences. They attribute this dependence to intrinsic defects induced during the manufacturing, which could have more influence on the thinnest laminates than on the thickest ones. Logically, thinner laminate specimens should show lower values of interlaminar tensile strength but Charrier et al. [24] highlight experimental results where thicker specimens have lower values of minimum strength. Hoffmann [25] points out test results where the thinnest specimens have the minimum strength, medium thickness specimens have the maximum strength and the thickest specimens have an intermediate interlaminar tensile strength. Avalon and Donaldson [26] present experimental results where the thickness dependence does not appear when no compressive fibre failure is observed. Kim et al. [27] and Fletcher et al. [28] show the importance of edge effects in the failure of the specimens. Premature failure can be induced by stress concentration close to the edges [29–32]. Pagano [33], O'Brien [34], and Lagunegrand et al. [35] demonstrate that edge effects cause local delamination on in-plane uniaxial tensile tests of unnotched specimens.

González-Cantero et al. [36] try to explain this thickness dependence of the interlaminar tensile strength by taking an alternative failure mechanism into account, where intralaminar failure occurs before the unfolding failure. This is explained by a high level of interlaminar tensile stress at the interface of adjacent layers and some intralaminar cracking, which reaches these interfaces, instantaneously causing crack delamination.

Sun and Kelly [37,38] then Martin and Jackson [39] introduced the idea that intralaminar matrix cracking appeared first and led to unfolding failure in cross-ply curved composite laminates, while traditional unfolding failure is considered to be caused by interlaminar stresses. More recently, Huchette et al. [40] used a Cohesive Zone Model to study the delamination onset from interlaminar damage in L-shaped specimens with a four-point bending test. They used specific stacking sequences to ensure matrix cracking before unfolding failure of the specimen. In the literature, some studies confirm that intralaminar cracks induce delamination in L-specimens with unidirectional plies: Sun and Kelly [37,38], Martin and Jackson [39], Michel et al. [41] and Huchette et al. [40].

In the first part of the present article, the “Discrete Ply Model” (DPM) is used to simulate the behavior up to failure of an L-shaped specimen. This approach was initially developed for impact simulations at the Institut Clément Ader [42–45] but was successfully extended to in-plane problems like open-hole tensile tests [46], scaling effects [47] or, more recently, to structural testing of large notches [48]. The four-point bending tests on L-angle specimens manufactured and tested experimentally by Charrier et al. [24,49] are taken. The ability of DPM to capture the load/machine displacement curves and the distribution of damage in the thickness of the specimens is accessed for different stacking sequences. Then the failure scenario is investigated to determine which damage drives the final failure. The influence of some discriminant parameters (frictional coefficient, transverse tensile and shearing strength, critical energy release rate (ERR) in modes I and II) is discussed.

2. Numerical modelling

In this section, the “Discrete Ply Model” (DPM) [42–48] is recalled very briefly. This model was initially developed to simulate impacts on composite structures and makes it possible to model various types of damage: delamination, matrix cracks and fibre breaks, during a failure scenario. This model has been more fully presented in previous papers and interested readers are invited to refer to them for more details. Then, the tests and specimen numerical modelling are detailed.

2.1. Modelling of various types of damage

The aim of the DPM is to simulate different failure modes of composite such as schematized in Fig. 1 by a complex 3D mesh following the orientation of each ply. The damage is modelled as follows:

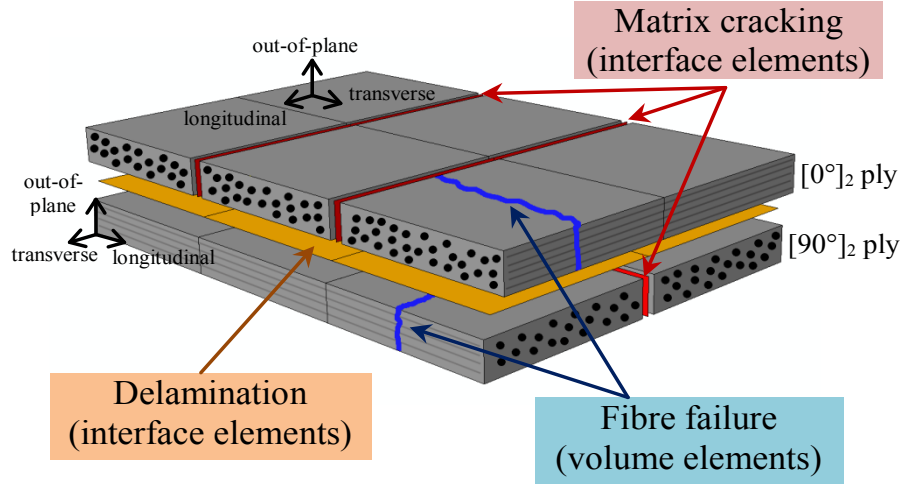


Fig. 1: DPM: modelling of damages

- The fibre failure is taken into consideration as a continuum damage inside the volume and is calculated at integration points of the element with a bilinear material law (Eq. 1) that considers the crack surface energy.

$$\int_V \left(\int_0^{\varepsilon^1} \sigma_l d\varepsilon_l \right) \cdot dV = S \cdot G_{Ic}^{fT} \quad (\text{Eq. 1})$$

where V and S are respectively the element volume and section, G_{Ic}^{fT} the critical energy release rate in opening mode in the fibre direction for the tensile case and G_{Ic}^{fC} for the compressive case, σ_l and ε_l the longitudinal stress and strain, and ε^1 the strain at total degradation of fibre stiffness.

When the strain threshold is achieved in tensile or compressive fibre failure, at ε_t^0 and ε_c^0 , respectively, a damage variable is used to apply a linear decrease in the calculation of the stress. Stresses are determined from the damaged orthotropic elastic stiffness matrix. In compression, a plastic behaviour and a crushing stress σ^{crush} [50] are also taken into consideration.

- Delamination is taken into account by using interface elements between consecutive plies (Fig. 1). Damage in delamination interface elements is managed by energy dissipation of fracture mechanisms. The delamination criterion is a linear coupling of three modes: the opening mode I and the transversal shear modes II and III. Modes II and III are not distinguished here. The criterion uses a linear law of mixed-mode delamination propagation with energy release in each mode (Eq. 2).

$$\frac{G_I}{G_{Ic}^{del}} + \frac{G_{II}}{G_{IIc}^{del}} + \frac{G_{III}}{G_{IIIc}^{del}} = 1 \quad (\text{Eq. 2})$$

- The matrix cracking is considered with interface elements between two juxtaposed volume elements, as illustrated in Fig. 1. The damage in matrix cracking interface elements is managed by Hashin's failure criterion, calculated in neighbouring volume elements (Eq. 3).

$$\left(\frac{\sigma_t^+}{\sigma_t^f}\right)^2 + \frac{\tau_{lt}^2 + \tau_{tz}^2}{(\tau_{lt}^f)^2} \leq 1 \quad (\text{Eq. 3})$$

where (l,t,z) are respectively for longitudinal, transverse and vertical directions, and σ_t^f and τ_{lt}^f are the transverse and the shear failure stresses, respectively.

2.2. Materials and boundary conditions

The aim of the four-point bending test is to induce a bending moment at the curved section created by the displacement of the two upper cylindrical bars, while the two lower ones stay fixed. Charrier et al. [24] studied the geometry of L-angle specimens (Fig. 2) to maximize the out-of-plane tensile stress and minimize the out-of-plane shear stress in the curved section in order to examine failure due to delamination. The dimensions of the specimens are reported in Table 1. Four different stacking sequences were manufactured:

- a unidirectional $[0_8]_s$ ply, noted UD,
- a quasi-isotropic $[(45/90/-45/0)_2]_s$ laminate, noted QI,
- a highly oriented $[0_3/45/90_2/-45/0]_s$ laminate, noted OR,
- a highly disoriented $[45_2/0/-45_3/90/45]_s$ laminate, noted DIS,

For more information about the choices of the L-angle specimen designs and the characteristic parameters of the experimental device for four-point bending tests, refer to [24].

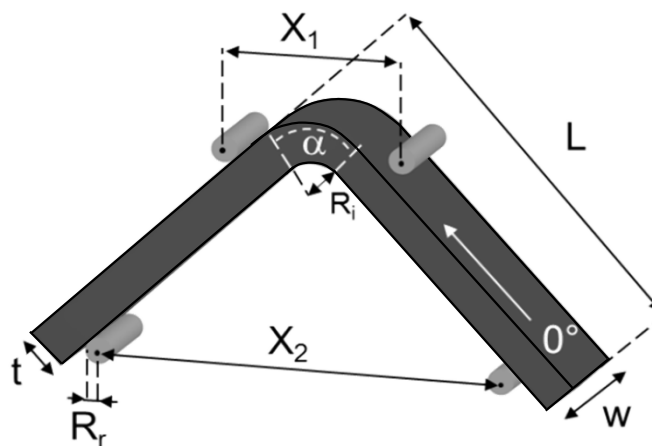


Fig. 2: Configuration of the four-point bending test on L-angle specimen [49]

Table 1: L-angle specimen nominal dimensions and characteristic parameters for the experimental device for four-point bending tests [49]

Thickness	Length	Width	Inner radius	Loading bars	Support bars
t (mm)	L (mm)	w (mm)	R_i (mm)	X_1 (mm)	X_2 (mm)
4.19	62	20	4	30	66

The DPM was used here to simulate these four-point bending tests on L-angle specimens of T700GC/M21 UD carbon/epoxy composite, as illustrated in Fig. 2. The nominal ply thickness was assumed equal to 0.262 mm. Properties used in the model are presented in Table 2. The number of plies varied between 16 for the UD stacking sequence and 9 for OR and DIS stacking sequences. Orientations were limited to 0° , $\pm 45^\circ$ and 90° to be comparable with experimental stacking sequences.

The entire specimen was meshed with the same sized elements and with one element per layer, except for the UD stacking sequence where there was one element per ply (thus 16 elements in the thickness). Models had from 220 000 to 400 000 elements and from 715 000 to 1 250 000 degrees of freedom. The computation time was between 6 and 13 hours. The volume elements used for fibre failure were C3D8 and C3D6 for all orientations. For delamination and matrix cracking, COH3D8 and COH3D6 elements were used. Each volume was enclosed by interface elements for matrix cracking in the direction of the ply as shown in Fig. 3 (in dark blue for the 90° and in dark green for the 45°). Interface elements used for delamination are not drawn on Fig. 3 because they were logically situated at the interface between two adjacent plies.

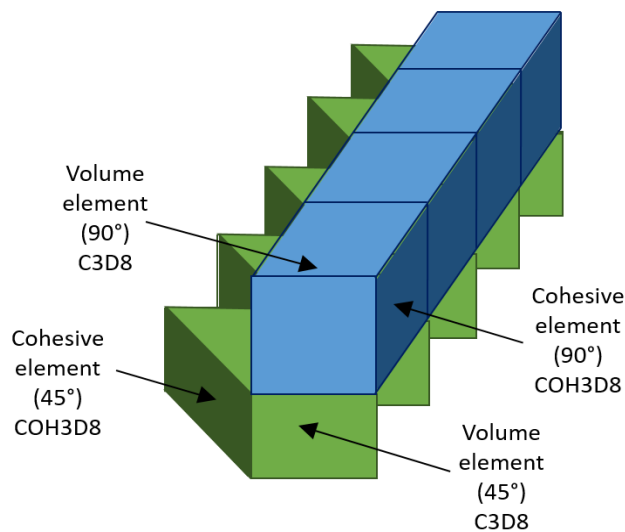


Fig. 3: Zoom on the mesh of specimen

Boundary conditions were applied on loading and support bars. Vertical displacements were applied on loading bars (the upper ones) and could rotate along the axis of the cylinder. Translations and rotation (except along the axis of the cylinder) were blocked for support bars (the lower ones).

Table 2: Material properties for DPM Modelling

Density		1 600 Kg/m ³
Orthotropic elastic properties		
E_l^t	Tensile Young's modulus in fibre direction	130 000 MPa
E_l^c	Compressive Young's modulus in fibre direction	100 000 MPa
E_t	Transverse Young's Modulus	7 700 MPa
G_{lt}	In-plane shear modulus	4 750 MPa
G_{tz}	Out-of-plane shear modulus	2 900 MPa
ν_{lt}	Poisson's ratio	0.3
Fibre failure		
σ^{crush}	Longitudinal compressive mean crushing stress	250 MPa
ε_t^0	Tensile strain in fibre direction at damage initiation	0.016
ε_c^0	Compressive strain in fibre direction at damage initiation	-0.0125
$G_{lc}^{f,T}$	Critical energy release rate in mode I for tensile case	100 N/mm
$G_{lc}^{f,C}$	Critical energy release rate in mode I for compressive case	40 N/mm
Delamination		
G_{lc}^{del}	Critical energy release rate in opening mode I	0.5 N/mm
G_{llc}^{del}	Critical energy release rate in transversal shear mode II	1.6 N/mm
Matrix cracking		
σ_t^f	Transverse tensile strength	50 MPa
τ_{lt}^f	In-plane shear strength	90 MPa

3. Experimental and numerical results of four-point bending tests on L-angle specimens

3.1. Results of ONERA four-point bending tests on the different stacking sequences

For each stacking sequence, the load and machine displacement at failure are summarized in Table

3.

Table 3: Load and machine displacement at failure (mean value and coefficient of variation, CV) of the different L-angle specimens subjected to four-point bending tests [49]

Thickness (mm)	UD		QI		OR		DIS	
	Load (N) (CV %)	Disp. (mm) (CV %)	Load (N) (CV %)	Disp. (mm) (CV %)	Load (N) (CV %)	Disp. (mm) (CV %)	Load (N) (CV %)	Disp. (mm) (CV %)
4.19	488 (7.9)	2.0 (6.3)	498 (2.7)	2.4 (4.1)	456 (2.7)	4.9 (0.7)	437 (4.8)	4.3 (2.5)

Charrier et al. [24] used finite element simulation to study distances between loading bars and support bars to minimize the out-of-plane shear stress and maximize the out-of-plane tensile stress as shown in Fig. 4. They did not want to induce additional out-of-plane shear stress close to the radius, which could cause premature failure. The out-of-plane shear stresses were negligible in the radius and the out-of-plane tensile stress was maximal at approximately one third of the thickness [24]. The load/machine displacement curves for all stacking sequences are plotted in Fig. 5. Each specimen showed a recovery of load after a first principal load drop. Both UD and OR specimens had a similar linear stiffness, of approximately 210 N/mm, and that of both QI and DIS specimens was approximately 90 N/mm. The load and the displacement at failure were similar for UD and OR specimens and for QI and DIS specimens.

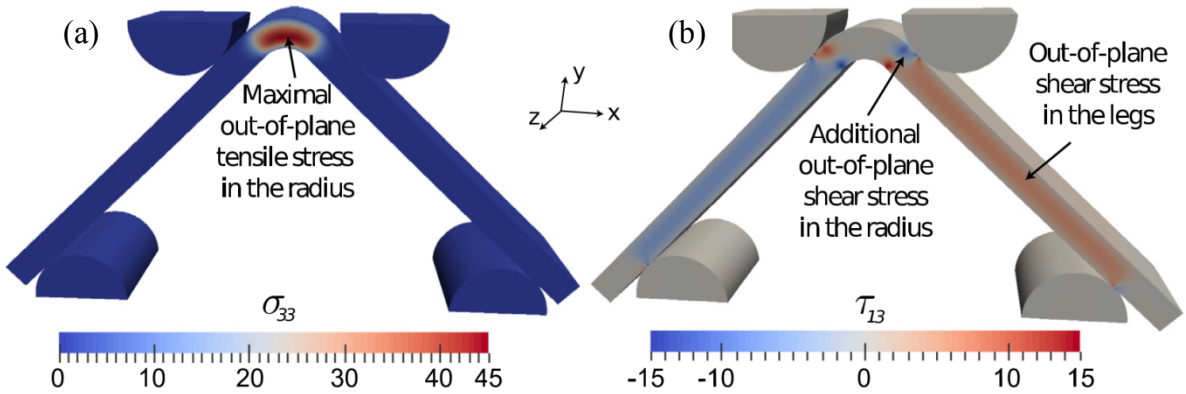


Fig. 4: Distribution of (a) out-of-plane tensile stress and (b) out-of-plane shear stress through the specimen [24]

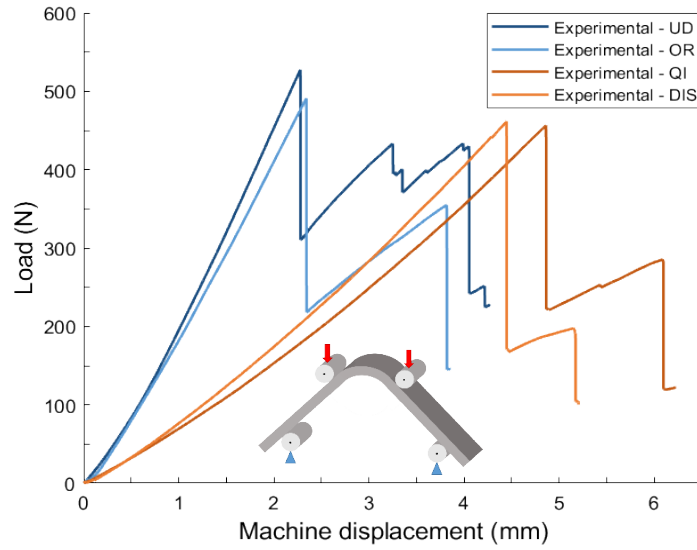


Fig. 5: Typical load/machine displacement curves for all stacking sequences studied

Two stacking sequences: DIS and OR are now studied more precisely. Fig. 6 and Fig. 7 represent the side faces for DIS and OR specimens, respectively. In Fig. 6, the presence of four delaminations between plies $[45_2/0]$, $[0/-45_3]$, $[-45_3/90]$ and $[90/45_2]$ can be observed. Matrix cracking within plies $[-45_3]$ and $[90]$ is also visible. Probably, damage was initiated by delamination and matrix cracking at $[90]$ ply level and caused the first load drop. Then damage spread through the thickness of the specimen and led to the second load drop at approximately 5 mm of machine displacement.

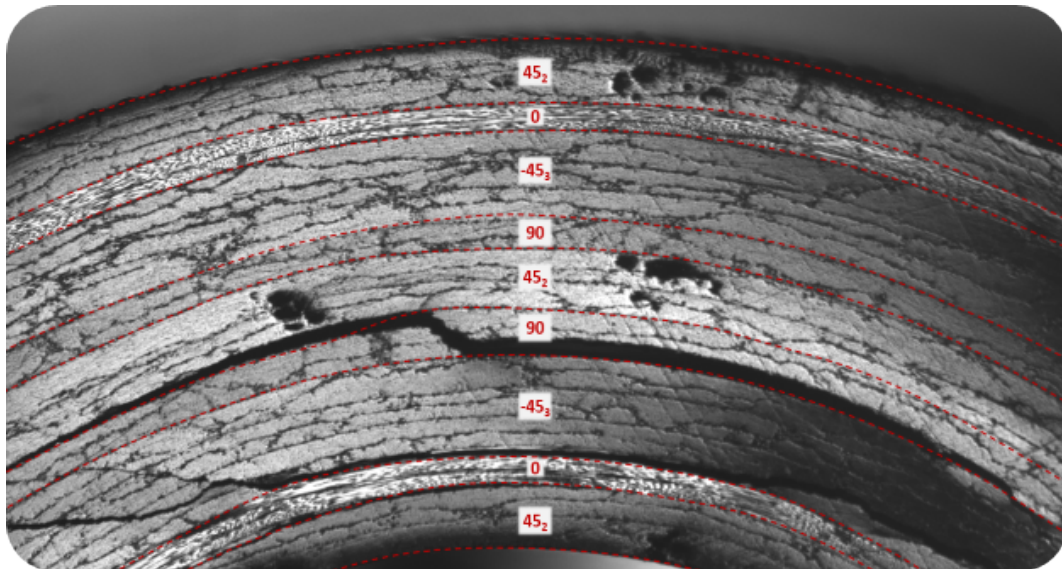


Fig. 6: Side face of DIS specimen at 460 N and 4.4 mm of displacement

In Fig. 7, two principal damage occurrences can be distinguished. The first is an in-the-ply sequence $[90_2/-45/0_2]$ with presence of matrix cracking in plies (90_2) and (-45) and delamination at the interface between plies $[-45/0_2]$. The second is localized in the ply sequence $[-45/90_2/45]$ where matrix cracking has occurred within the central ply (90_2) and delaminations around it. The first damage initiated occurs lower in the stacking sequence, appearing at 480 N and 2.3 mm of machine displacement. It is probable that this damage induced the first load drop and the upper damage induced the second load drop at 380 N and 3.9 mm of machine displacement. Matrix cracking and delaminations are seen to be present in both cases.

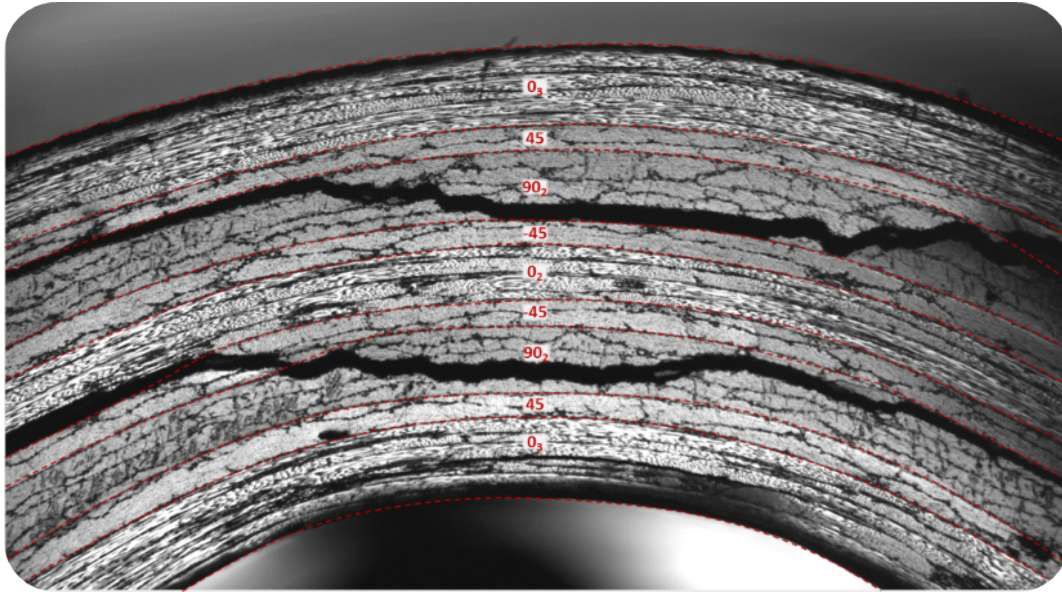


Fig. 7: Side face of OR specimen at 380 N and 3.9 mm of displacement

3.2. Numerical result of four-point bending test

3.2.1. DIS specimen

The FE simulation with the DPM showed good agreement with experimental results (Fig. 8 (a)). Stiffness (107 N/mm), maximal load (483 N) and machine displacement at failure (4.1 mm) were close to the experimental results. The DPM model also revealed where the different damage occurrences were localized, which types of damage induced different load drops and which induced the final failure of the specimen. Fig. 8 (b) summarizes the failure scenario of the DIS specimen with the damage of matrix cracking extending into every layer and delamination at each interface, for a displacement of 4.2 mm illustrated by the red point on the load/displacement curve. The damage that caused the load drop was the delamination between layers 2 and 3, corresponding to the interface between plies $(0/-45_3)$, represented by the first red lines on Fig. 9. Two other delaminations were due to the load drop: delamination between layers 3/4 and between layers 4/5, corresponding to interfaces between plies $(-45_3/90)$ and $(90/45_2)$,

respectively, represented by the other two red lines on Fig. 9. The model shows that a huge proportion of the specimens failed. Damage extended to layer n°7, which corresponds to the -45_3 ply (Fig. 9). The two numerical side faces were different, indicating that some damage did not come out on the external faces. In the experimental tests, there was no damage above the interface (4/5), corresponding to the interface between plies ($90/45_2$). This can be explained by the fact that delamination and matrix cracking can be localized within the width of the specimen. It can also explain the difference of load reaction, between experimental and numerical, on the load/machine displacement graph. The numerical damage may have been spread too abruptly, which would explain why the drop was too large compared to the experimental one, and the presence of damage above the interface (4/5).

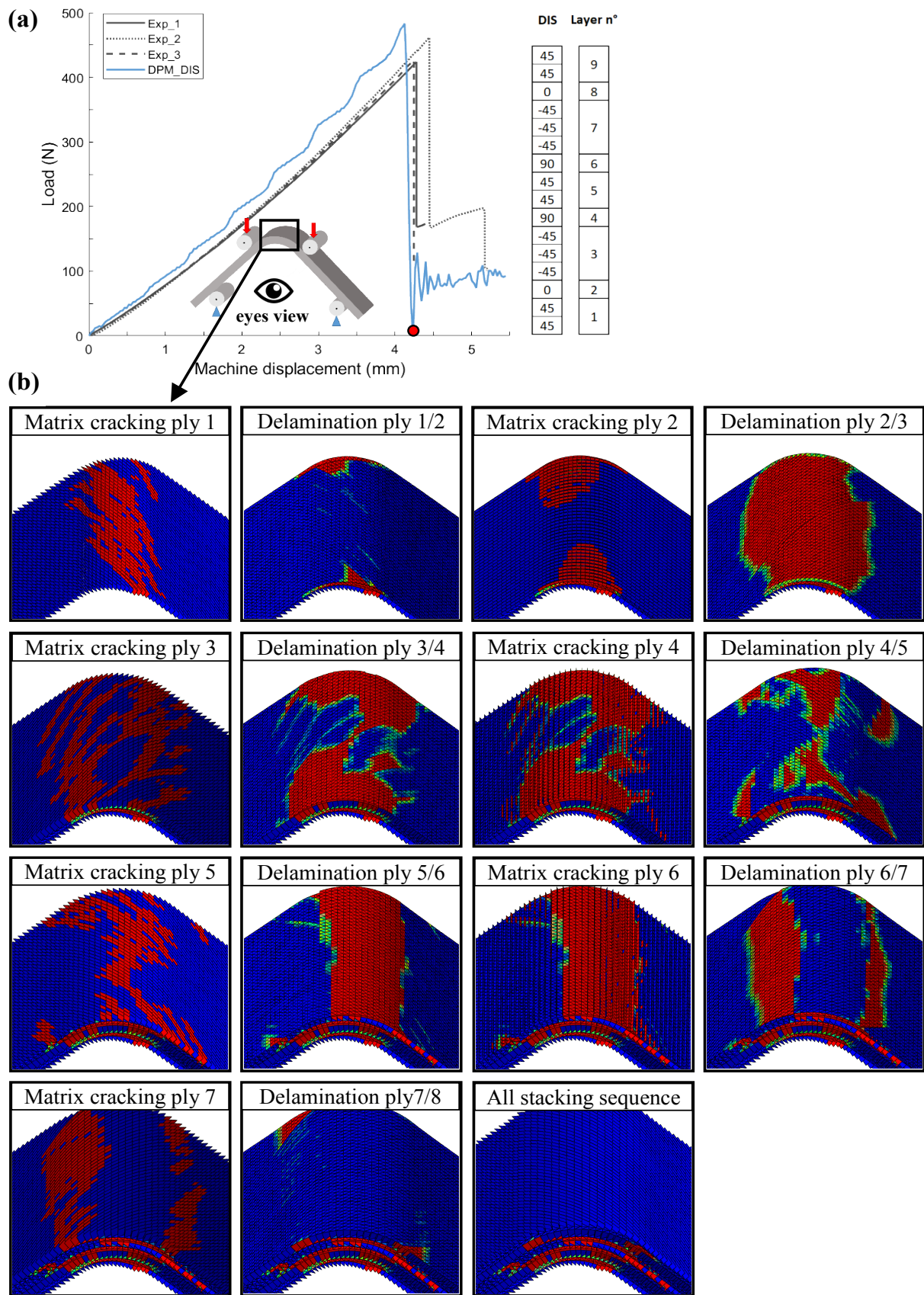


Fig. 8: (a) Comparison between experimental and DPM load/displacement curves of DIS specimen and (b) breaking scenario of DIS specimen with matrix cracking and delamination for each layer

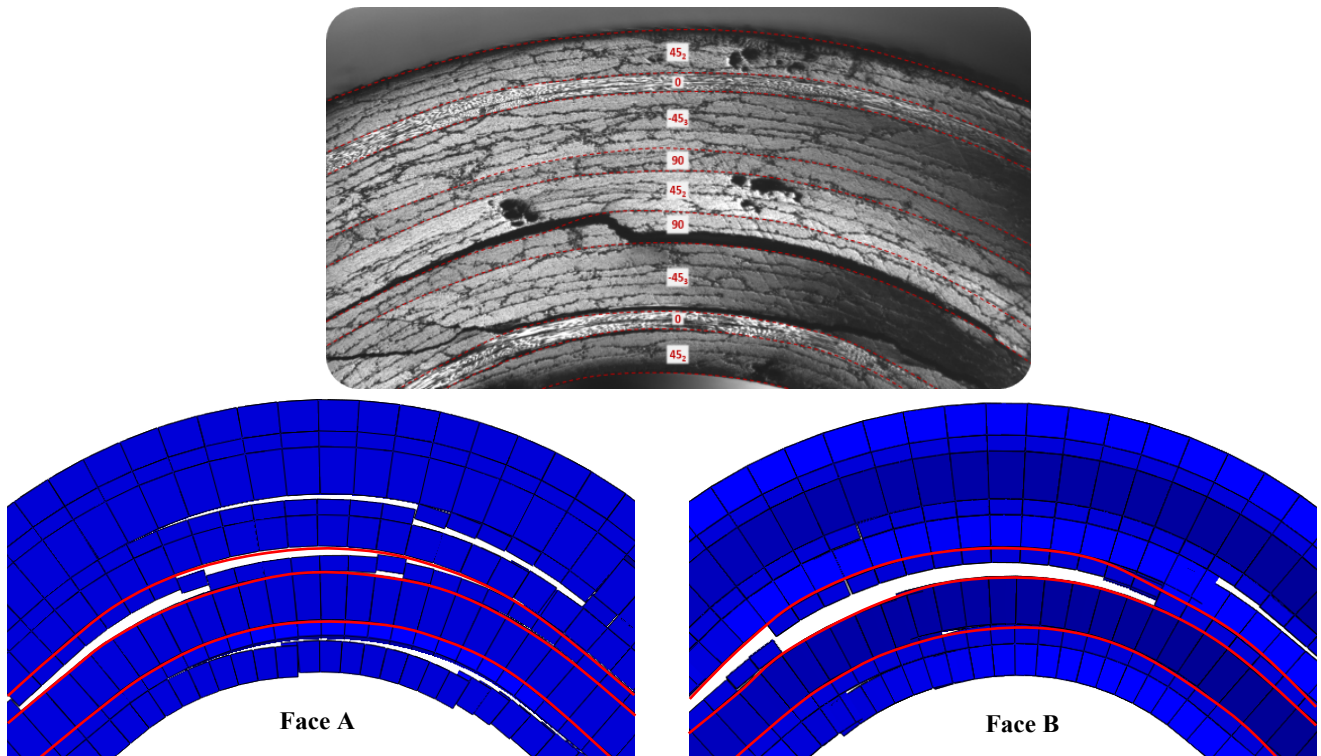


Fig. 9: Experimental and numerical side faces of DIS specimen after failure

3.2.2. QI specimen

Fig. 10 shows that the numerical stiffness was very close to the experimental one. However, the load at failure was approximately 50 N higher than that measured experimentally. In the same way as for the previous specimen, the load drop was too large compared to experimental curves, except for the third experimental curve, which did not exhibit a load drop. The simulation achieved the level of the last load drop directly, without finding the intermediate one at 200 N. As for the DIS specimen, this can be explained by the damage spreading too abruptly into the thickness of the specimen. The failure of L-angle specimens under four-point bending tests is instantaneous and, in some cases, not easily repeatable.

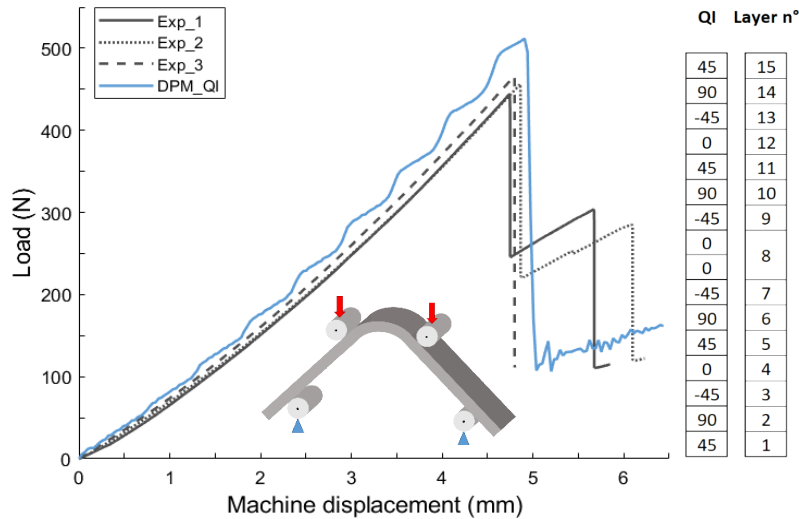


Fig. 10: Comparison between experimental and DPM load/machine displacement curves of QI specimen

3.2.3. OR specimen

The four-point bending test on this specimen, with the OR stacking sequence, was a little different from the two tested previously. It presented a premature rupture at approximately 510 N and 2.3 mm of machine displacement, with a load reaction spread out over 1.5 mm of machine displacement before the second load drop. Very good agreement was found between experimental and FE simulation (Fig. 11 (a)). The model allows the type and localization of damage to be examined for each load drop. After the first one, the model showed damage extending to layer n° 4, corresponding to (-45) (Fig. 11 (b)). This first decrease of effort was driven by the delamination between layers (1/2), corresponding to plies (0₃/45). Two other delaminations drove the first load drop, between layers (2/3) and (3/4), corresponding to interfaces (45/90₂) and (90₂/-45), respectively, as shown in Fig. 11. The second load drop was due to the delamination at the interface between layers (5/6), (6/7) and (7/8), respectively corresponding to interfaces (0₂/-45), (-45/90₂) and (90₂/45) in Fig. 12. This was related with the fact that, experimentally, there were two load drops as presented in part 3.1. The first load drop was driven by damage in the lower part of the specimen and the second by damage in the upper part (Fig. 7).

Numerically, the same pattern as the experimental one was found, with damage located at the same level in the thickness of the specimen (Fig. 13). So, the model succeeded in capturing the failure scenario.

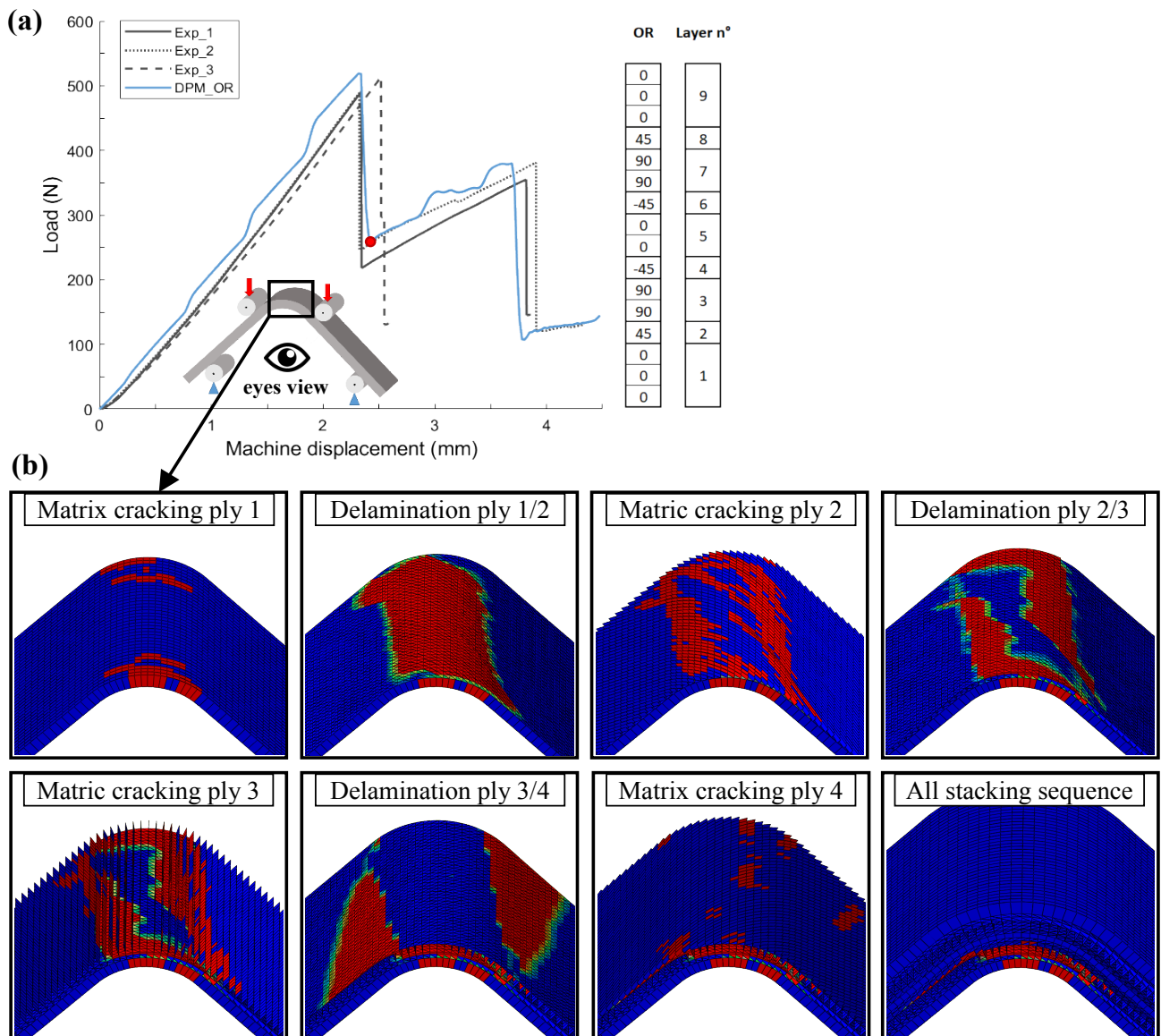


Fig. 11: (a) Comparison between experimental and DPM load/displacement curves of OR specimen and (b) breaking scenario of OR specimen with matrix cracking and delamination for each layer at the first load drop (2.5 mm of machine displacement)

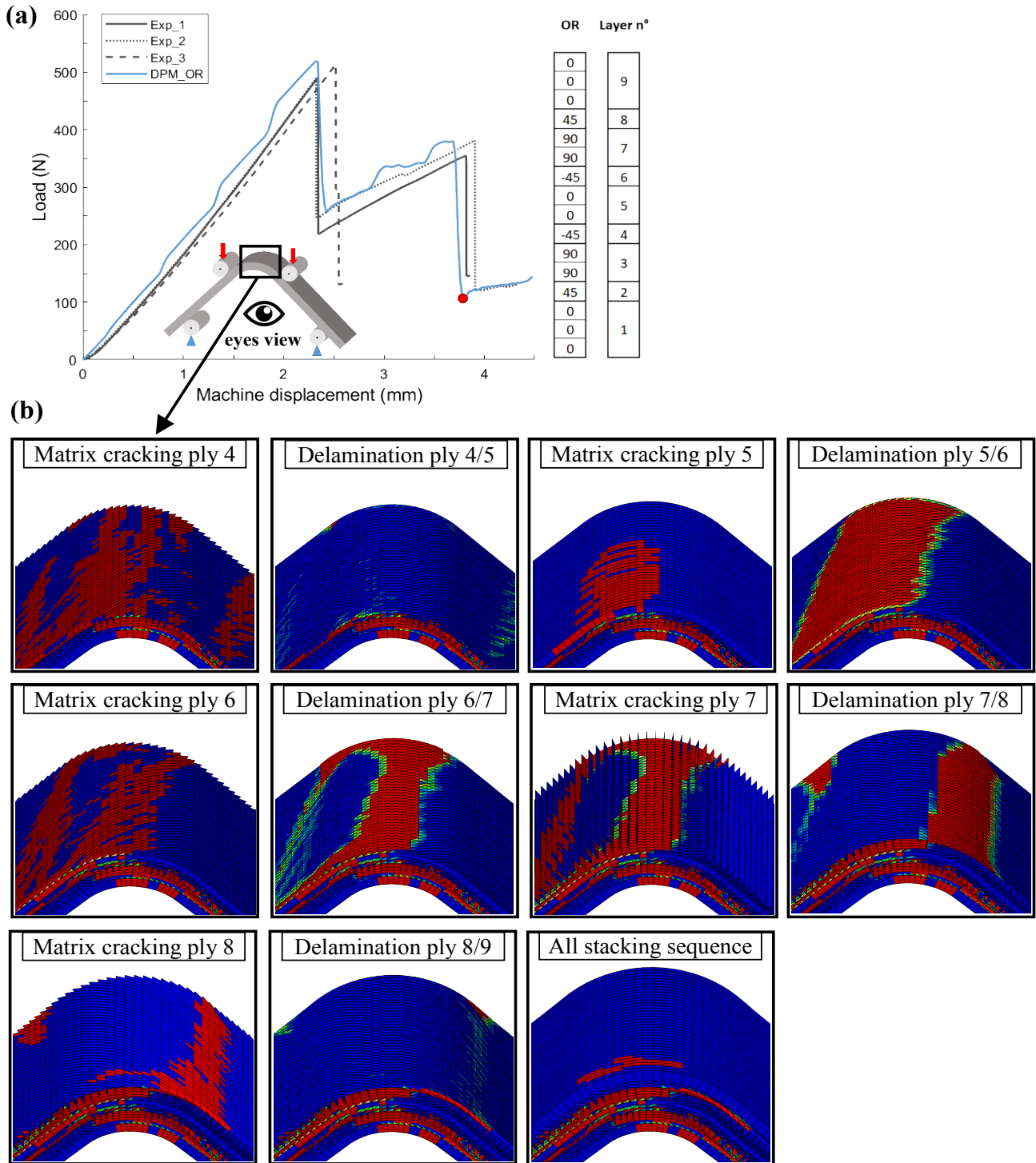


Fig. 12: (a) Comparison between experimental and DPM load/machine displacement curves of OR specimen and (b) breaking scenario of OR specimen with matrix cracking and delamination for each layer at the second load drop (3.8 mm of machine displacement)

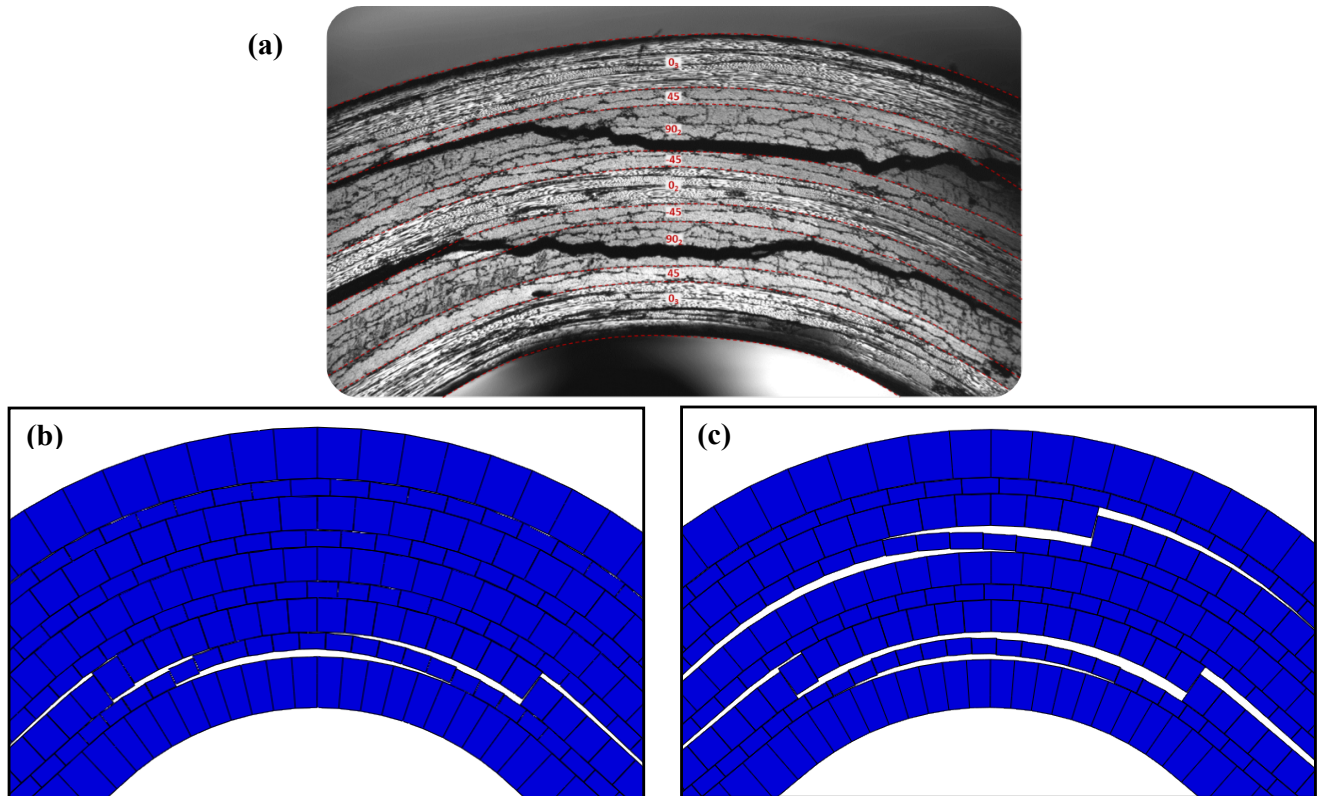


Fig. 13: (a) Numerical side face of OR specimen at the first load drop (2.5 mm of machine displacement), (b) at the second load drop (3.8 mm of machine displacement)

3.2.4. UD specimen

For the UD stacking sequence, one element was used per layer for sixteen plies, implying a total of fourteen interfaces between layers. This last FE simulation of the four-point bending test on a UD specimen was comparable to the previous ones. Very similar overall behaviour was found with the same initial stiffness and some loads reacting after the first load drop (see Fig. 14). The first load drop, at approximately 2.0 mm of machine displacement, was caused by delamination between layers (5/6) and (6/7) and the second load drop, at 2.5 mm of machine displacement, was induced by delamination between layers (2/3), (9/10) and (10/11).

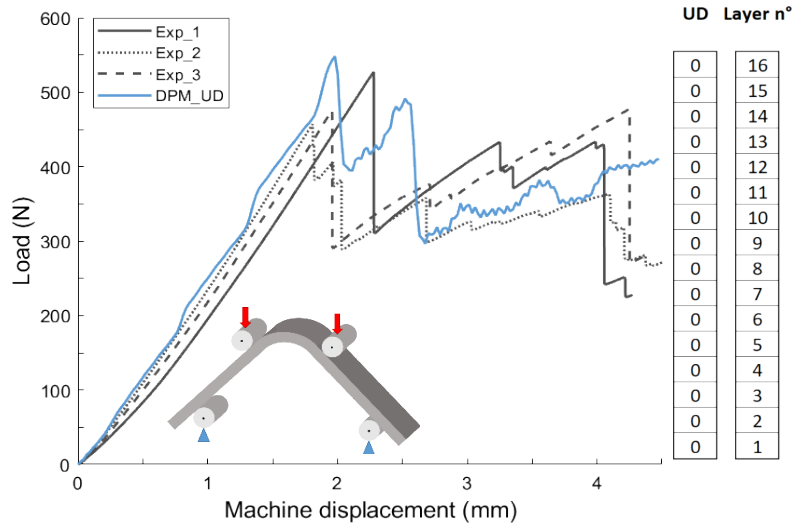


Fig. 14: Comparison between experimental load/machine displacement curves and DPM load/machine displacement curves of UD specimen

4. Sensitivity analysis

The present section proposes to study the influence of different parameters on the load/machine displacement curves and their impact on the scenario of rupture according to DPM modelling. This section firstly describes the influence of the friction coefficient for different stacking sequences, secondly describes the influence of the modelling strategy (by modelling the translaminar matrix cracking or not) and thirdly studies material parameters such as the transverse tensile and shearing strengths, and the critical ERR in modes I and II.

4.1. Influence of frictional coefficient

FE simulations were carried out on each stacking sequence with three different values of frictional coefficients: 0, 0.15 and 0.3. These simulations highlight a marked effect of the frictional coefficient on the stiffness of specimen and on the maximum load before the first load drop. Increasing the frictional coefficient raised the stiffness, of the maximum load and of the displacement at failure, as shown in Fig. 15. The impact of the frictional coefficient was independent of the specimen and had no consequence on the load reaction that appeared after the main load drop.

Therefore, it is really important to use a test configuration with cylindrical bars mounted on roller bearings to minimize the frictional coefficient between the cylindrical bars and the specimen to ensure a good restitution of effort, as mentioned in the ASTM standard [51].

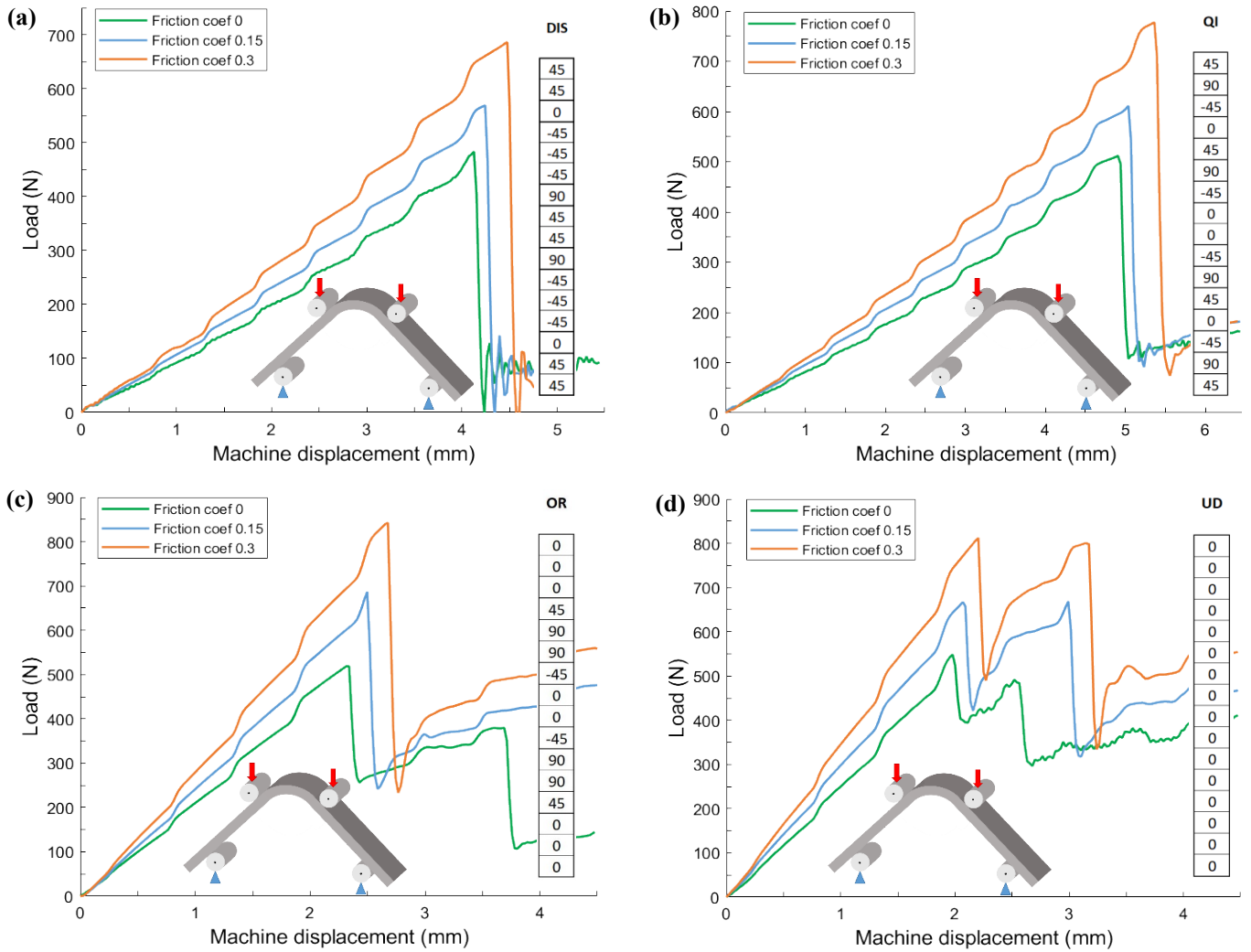


Fig. 15: Comparison between load/machine displacement curves for different friction coefficient values (0, 0.15 and 0.3): (a) of DIS specimen; (b) of QI specimen; (c) of OR specimen and (d) of UD specimen

4.2. Modelling the influence of intralaminar matrix cracking

The influence of an intralaminar matrix crack depended on the stacking sequence as shown in Fig. 16 and Fig. 17. For the DIS specimen, the fact that intralaminar matrix cracking was not considered in the simulation caused a delay in the failure of the specimen. Nevertheless, delamination was displaced by just one interval of interface with respect to the reference DPM_DIS. On the reference simulation with the DPM, it was the second interface (between plies 0/-45₃) of the inner radius that delaminated first. On the FE simulation without matrix cracking, it was the third interface (between plies -45₃/90) that failed first and it was the only one. Both failures corresponded to delamination present experimentally, so it was impossible to affirm which one broke first in the experiment. Notwithstanding, intralaminar matrix cracking is necessary to propagate damage through the thickness of the specimen. This is consistent with the hypothesis made by Sun and Kelly [37,38], Martin and Jackson [39], Michel et al. [41], Huchette et al. [40]

and González-Cantera et al. [36], who think that an intralaminar crack introduces the delamination onset and propagates instantaneously causing the final failure of the test piece.

For the other specimen, with the OR stacking sequence, not considering intralaminar matrix cracking did not show an influence on the load and machine displacement at failure (Fig. 17) or on the first interface to delaminate. In both simulations, the first interface to delaminate was between plies (0₃/45). For the reference DPM_OR, interfaces between plies (45/90₂) and (90₂/-45) broke in addition to the previous one. For the simulation without matrix cracking, delamination of the interface (90₂/-45) appeared with the previous one between plies (0₃/45) and corresponded to the first load drop. A difference was noted on the main load drops between the two simulations. The one without translaminar matrix cracking showed a smaller load drop than the others. This can be explained by the fact that three interfaces failed on the reference DPM_OR simulations and just two on the simulation without translaminar matrix cracking, so the gap was reduced.

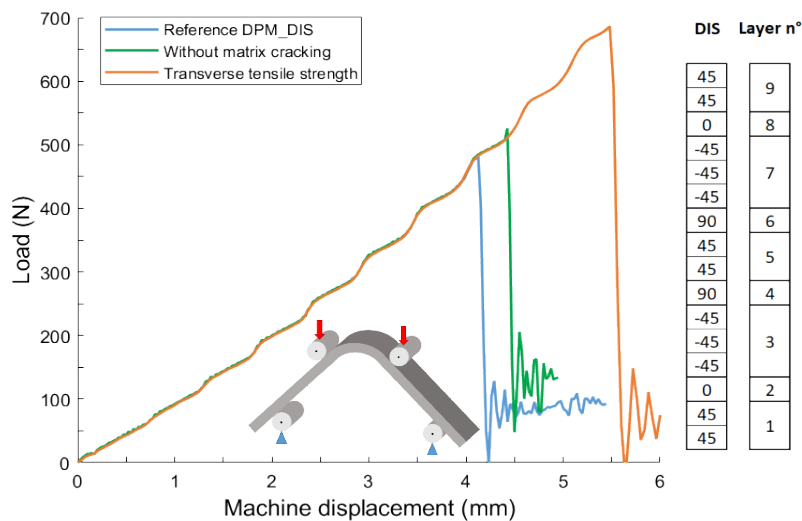


Fig. 16: Comparison between load/machine displacement curves for different discriminating parameters of DIS specimen

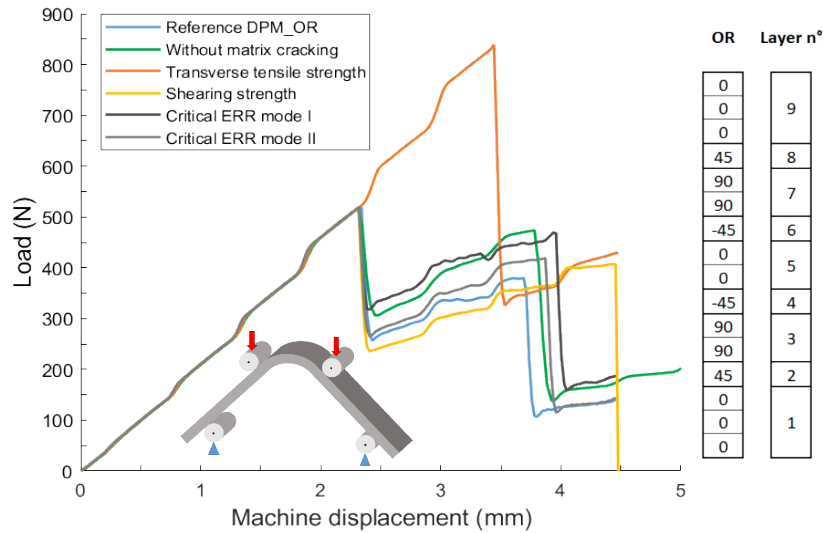


Fig. 17: Comparison between load/machine displacement curves for different discriminating parameters of OR specimen

4.3 Influence of material properties

Impact of transverse tensile strength on simulations

To study the impact of the transverse tensile strength (used in the calculation of the matrix cracking and the delamination) during the four-point bending test, the transverse tensile strength was increased by 50%. In both cases, the moment of the principal failure of specimens shifted. The load at failure increased by 42% and 62% respectively for the DIS and OR specimens and the displacement at failure increased by 34% and 48%. This is in harmony with the coefficient of 50% applied to the transversal tensile strength. This leads us to state that the principal failure is driven by the transversal tensile strength in these cases, which corresponds to out-of-plane tensile stresses, and is consistent with the works of Charrier et al. [24], who tried to maximize the out-of-plane tensile stress and minimize the out-of-plane shear stress. For both stacking sequences, damage was similar to that of the reference cases. The first layer to delaminate was the same but the propagation of failures into the specimen was quicker than for reference cases (DPM_DIS and DPM_OR). The high sensitivity to this parameter should indicate to designers that the strength of this kind of parts can be enhanced by selective stitching or Z-Pinning.

Influence of shearing strength and critical energy release rate in modes I and II

In the case of DIS specimens, applying a coefficient of 50% on shearing strength, and critical energy release rate in modes I and II, surprisingly, had no influence on load/machine displacement curves, which is why these curves are not drawn on Fig. 16. We thus conclude that this test was principally driven by the matrix cracking, which is in line with recent literature [36].

For the OR specimen (Fig. 17), a limited effect was observed. Shear strength did not modify the first part of the curve, until the first drop. The load reaction was longest and the second load drop occurred

approximately 1.3 mm later than for the reference case. This suggests that the second load drop is driven by the shearing stress. Concerning the ERR in modes I and II, mode II had a weak impact compared to the reference case on the OR stacking sequence. The influence of the critical energy release rate in mode I had an effect on the load/machine displacement curve that was similar to the simulation not taking the intralaminar matrix cracking into consideration. These simulations lead us to think that the critical ERR in mode I has more impact on damage propagation than the critical energy release rate in mode II.

5. Conclusions

Four-point bending tests on L-angle specimens create a bending moment in the highly curved laminates of the specimen, which induces critical out-of-plane tensile stress concentration in the part where the curvature is strong and leads to unfolding failure. Generally speaking, the unfolding failure is attributed to delamination. Thanks to the “Discrete Ply Model”, numerically more complex failure scenarios have been shown for four typical stacking sequences and, more particularly, for DIS and OR. In addition, DPM allows the influence of different parameters on the simulation to be estimated independently, which is the key point of the model and the only way to make this study possible.

DPM gives good agreement between experimental and numerical simulations, especially for the restitution of load/machine displacement curves and the damage pattern of the specimen tested. The model finds the maximal load, load drops and the different reaction loads with good agreement for the four stacking sequences studied.

In the case of the DIS stacking sequence, intralaminar matrix cracking appears before the first delamination but does not lead to the final failure of the specimen. Nevertheless, when matrix cracking is not modelled, the load drop is found for a greater displacement than experimentally. Moreover, the variation of shearing strength and critical ERR in modes I and II has no impact on load/machine displacement curves.

For the OR specimen, no intralaminar matrix cracking is found before the first delamination. All damage appears at the same time and it is delamination, which leads to final failure. This was demonstrated by running a simulation that did not model matrix cracking. This simulation shows a first load drop consistent with the test displacements. Only the reacting load and the second load drop are modified. So, matrix cracking drives the test and allows damage to propagate through the thickness of the specimen but the final failure is due to delamination.

In this study, the influence of the frictional coefficient on the response of the model, and in particular on the stiffness, was pointed out. Increasing the frictional coefficient increases the stiffness of the model

and therefore the maximum load and the displacement at failure. These results are consistent with the literature [36–39].

The influence of intralaminar matrix cracking was studied by running specific simulations that did not model it. When this was done, DIS and OR specimens exhibited significant differences. In the case of the DIS stacking sequence, the intralaminar matrix cracking caused a delay in the appearance of the main load drop. It allowed damage to spread into the thickness of the part.

It was also shown that interply tensile and shear strength and critical energy release rate in modes I and II had a visible but low impact on the OR stacking sequence, and no significant influence for the other stackings. Their influence intervened just after the main load drop. Notwithstanding, delaminations were mostly propagated in mode I rather than in mode II.

Finally, the DPM modelling strategy was able to demonstrate the influence of matrix transverse tensile strength and to show that it drives the failure of the parts tested on both DIS and OR specimens. Unfolding failure is a complex mechanism driven by delamination (in mode I) but intralaminar matrix cracking is also necessary to give good agreement with experimental results.

References

- [1] Paul PC, Saff CR, Sanger KB, Mahler MA, Kan HP, Kautz EF. Out of plane analysis for composite structures. NASA Tech Report, NASA Langley Res Center, Eighth DOD(NASA)FAA Conf Fibrous Compos Struct Des Part 1; P 263-279 1995:263–79.
- [2] Kedward KT, Wilson RS, McLean SK. Flexure of simply curved composite shapes. *Composites* 1989;20:527–36. doi:10.1016/0010-4361(89)90911-7.
- [3] Lekhnitskii SG, Tsai SW, Cheron T. *Anisotropic Plates*. Gordon and Breach Science Publishers; 1968.
- [4] Ko L. Delamination stresses in semicircular composite laminated bars. 4026, 1988.
- [5] Sharma A, Bakis CE. Analysis of elastic stresses in thick, polar-orthotropic, C-shaped rings. *J Compos Mater* 2004;38:1619–38. doi:10.1177/0021998304043888.
- [6] Sharma A, Bakis CE. C-shape specimen for tensile radial strength of thick, filament-wound rings. *J Compos Mater* 2006;40:97–116. doi:10.1177/0021998305053505.
- [7] Schmitz A, Horst P. Bending deformation limits of corrugated unidirectionally reinforced composites. *Compos Struct* 2014;107:103–11. doi:10.1016/j.compstruct.2013.07.048.

- [8] Ko L, Jackson RH. Multilayer Theory for Delamination Analysis of a Composite Curved Bar Subjected to End Forces and End Moments. 4139, 1989. doi:10.1007/978-94-009-1125-3_7.
- [9] González-Cantero JM, Graciani E, Blázquez A, París F. A new analytical model for evaluating interlaminar stresses in the unfolding failure of composite laminates. *Compos Struct* 2016;147:260–73. doi:10.1016/j.compstruct.2016.03.025.
- [10] Most J, Stegmair D, Petry D. Error estimation between simple, closed-form analytical formulae and full-scale FEM for interlaminar stress prediction in curved laminates. *Compos Struct* 2015;131:72–81.
- [11] González-Cantero JM, Graciani Díaz E, París F, López-Romano B, Meizoso Latova D. Semi-analytic solution on non-regularized unfolding stress in composite beams employing a series approximation based on legendre polynomials, Copenhagen, Denmark: 2015.
- [12] González-Cantero JM, Graciani E, París F, López-Romano B. Semi-analytic model to evaluate non-regularized stresses causing unfolding failure in composites. *Compos. Struct.*, vol. 171, 2017, p. 77–91. doi:10.1016/j.compstruct.2017.02.016.
- [13] Orifici AC, Herszberg I, Thomson RS. Review of methodologies for composite material modelling incorporating failure. *Compos Struct* 2008;86:194–210. doi:10.1016/j.compstruct.2008.03.007.
- [14] Kim R, Soni S. Failure of composite laminates due to combined interlaminar normal and shear stresses. *Proc. Japan-US CCM-III*, 1986, p. 341–50.
- [15] Brewer JC, Lagace PA. Quadratic Stress Criterion for Initiation of Delamination. *J Compos Mater* 1984;22:1141–55. doi:10.1177/002199838802201205.
- [16] Wisnom MR, Hill GFJ, Jones M. Through thickness failure prediction of composite structural elements. *ICCM-13*, n.d.
- [17] ASTM D 2344/D 2344M -13, Standard Test Method for Short-beam Strength of Polymer Matrix Composite Materials and Their Laminates n.d.
- [18] ASTM D6415/D 6415M -06a, Standard test method for measuring the curved beam strength for fiber reinforced polymer matrix composite n.d.
- [19] Jackson WC, Ifju P. Through-the-thickness tensile strength of textile composites. *Compos Mater Test Des* 1996;12:218–38.
- [20] Makeev A, Seon G, Nikishkov Y, Lee E. Methods for assessment of interlaminar tensile strength

- of composite materials. *J Compos Mater* 2015;49:783–94. doi:10.1177/0021998314525979.
- [21] ASTM D7291 / D7291M -15, Standard test method for through-thickness “flatwise” tensile strength and elastic modulus of a fiber-reinforced polymer matrix composite material n.d.
- [22] Hoffmann M, Zimmermann K, Bautz B, Middendorf P. A new specimen geometry to determine the through-thickness tensile strength of composite laminates. *Compos. Part B Eng.*, vol. 77, Elsevier Ltd; 2015, p. 145–52. doi:10.1016/j.compositesb.2015.03.020.
- [23] Edwards T, Thompson J. Spar Corner Radius Integrity for the A400M Wing. *Appl Mech Mater* 2005;3-4:197–204. doi:10.4028/www.scientific.net/amm.3-4.197.
- [24] Charrier JS, Laurin F, Carrère N, Mahdi S. Determination of the out-of-plane tensile strength using four-point bending tests on laminated L-angle specimens with different stacking sequences and total thicknesses. *Compos Part A Appl Sci Manuf* 2016;81:243–53. doi:10.1016/j.compositesa.2015.11.018.
- [25] Hoffmann M, Zimmermann K, Bautz B, Middendorf P. Size effect on through thickness strength properties of 3D loaded composite laminates. ECCM-17, Munich, Germany: 2016.
- [26] Avalon SC, Donaldson SL. Strength of composite angle brackets with multiple geometries and nanofiber-enhanced resins. *J Compos Mater* 2011;45:1017–30. doi:10.1177/0021998310381538.
- [27] Kim T, Fletcher TA, Dodwell TJ, Butler R, Scheichl R, Ankersen J, et al. The effect of free edges on inter-laminar performance of curved laminates. AIAA/ASCE/AHS/ASC, Structures; Struct. Dyn. Mater. Conf., 2015, p. 1. doi:10.2514/6.2015-0968.
- [28] Fletcher TA, Kim T, Dodwell TJ, Butler R, Scheichl R, Newley R. The Influence of Free Edges on Curved Beam Strength. ICCM-20, Copenhagen: 2015.
- [29] Kitching R, Tan AL, Abu-Mansour TMN. The influence of through thickness properties on glass reinforced plastic laminated structures. *Compos Struct* 1984;2:105–51. doi:10.1016/0263-8223(84)90024-2.
- [30] Hodgkinson J, Ayache S, Matthews F. In-plane and out-of-plane property measurements on thick woven glass/polyester laminates. ECCM-5, Amsterdam, Netherlands: 1992.
- [31] Hara E, Yokozeki T, Hatta H, Ishikawa T, Iwahori Y. Effects of geometry and specimen size on out-of-plane tensile strength of aligned CFRP determined by direct tensile method. *Compos Part A Appl Sci Manuf* 2010;41:1425–33. doi:10.1016/j.compositesa.2010.06.003.

- [32] Hara E, Yokozeki T, Hatta H, Iwahori Y, Ishikawa T. Comparison of out-of-plane tensile moduli of CFRP laminates obtained by 3-point bending and direct loading tests. *Compos Part A Appl Sci Manuf* 2014;67:77–85. doi:10.1016/j.compositesa.2014.08.003.
- [33] Pagano NJ. Free edge stress fields in composite laminates. *Int J Solids Struct* 1978;14:401–6. doi:10.1016/0020-7683(78)90021-5.
- [34] O'Brien TK. Characterization of delamination onset and growth in a composite laminate, 1981.
- [35] Lagunegrand L, Lorriot T, Harry R, Wagnier H, Quenisset JM. Initiation of free-edge delamination in composite laminates. *Compos Sci Technol* 2006;66:1315–27. doi:10.1016/j.compscitech.2005.10.010.
- [36] González-Cantero JM, Graciani E, López-Romano B, París F. Competing mechanisms in the unfolding failure in composite laminates. *Compos Sci Technol* 2018;156:223–30. doi:10.1016/j.compscitech.2017.12.022.
- [37] Sun CT, Kelly SR. Failure in Composite Angle Structures Part I: Initial Failure. *J Reinf Plast Compos* 1988;7:220–32. doi:10.1177/073168448800700302.
- [38] Sun CT, Kelly SR. Failure in Composite Angle Structures Part II: Onset of Delamination. *J Reinf Plast Compos* 1988;7:233–44. doi:10.1177/073168448800700302.
- [39] Martin H, Jackson WC. Damage prediction in cross-ply curved composite laminates, 1991.
- [40] Huchette C, Vandellos T, Laurin F. *Damage Growth in Aerospace Composites*. Springer; 2015. doi:10.1007/978-3-319-04004-2.
- [41] Michel L, Garcia S, Yao C, Espinosa C, Lachaud F. Experimental and Numerical Investigation of Delamination in Curved-Beam Multidirectional Laminated Composite Specimen. *Key Eng Mater* 2013;577-578:389–92. doi:10.4028/www.scientific.net/kem.577-578.389.
- [42] Bouvet C, Castanié B, Bizeul M, Barrau JJ. Low velocity impact modelling in laminate composite panels with discrete interface elements. *Int J Solids Struct* 2009;46:2809–21. doi:10.1016/J.IJSOLSTR.2009.03.010.
- [43] Bouvet C, Rivallant S, Barrau JJ. Low velocity impact modeling in composite laminates capturing permanent indentation. *Compos Sci Technol* 2012;72:1977–88. doi:10.1016/J.COMPSCITECH.2012.08.019.
- [44] Hongkarnjanakul N, Bouvet C, Rivallant S. Validation of low velocity impact modelling on

different stacking sequences of CFRP laminates and influence of fibre failure. *Compos Struct* 2013;106:549–59. doi:10.1016/j.compstruct.2013.07.008.

- [45] Dubary N, Bouvet C, Rivallant S, Ratsifandrihana L. Damage tolerance of an impacted composite laminate. *Compos Struct* 2018;206:261–71. doi:10.1016/J.COMPSTRUCT.2018.08.045.
- [46] Achard V, Bouvet C, Castanié B, Chirol C. Discrete ply modelling of open hole tensile tests. *Compos Struct* 2014;113:369–81. doi:10.1016/j.compstruct.2014.03.031.
- [47] Serra J, Bouvet C, Castanié B, Petiot C. Scaling effect in notched composites: The Discrete Ply Model approach. *Compos Struct* 2016;148:127–43. doi:10.1016/j.compstruct.2016.03.062.
- [48] Serra J, Pierré J-E, Passieux J-C, Périé J-N, Bouvet C, Castanié B, et al. Validation and modeling of aeronautical composite structures subjected to combined loadings: The VERTEX project. Part 2: Load envelopes for the assessment of panels with large notches. *Compos Struct* 2017;180:550–67. doi:10.1016/j.compstruct.2017.08.055.
- [49] Charrier JS. Développement de méthodologie dédiées à l'analyse robuste de la tenue de structures composites sous chargements complexe tridimensionnels. 2013.
- [50] Israr HA, Rivallant S, Barrau JJ. Experimental investigation on mean crushing stress characterization of carbon–epoxy plies under compressive crushing mode. *Compos Struct* 2013;96:357–64. doi:10.1016/J.COMPSTRUCT.2012.09.022.
- [51] ASTM D 6415 - Standard Test Method for Measuring the Curved Beam Strength of a Fiber-Reinforced Polymer-Matrix Composite n.d.